

Stress-Strain Data Obtained at High Rates Using an Expanding Ring

Investigation indicates that dynamic symmetrical free expansion of thin rings offers a valid means for obtaining uniaxial tensile stress-strain relationships at high strain rates

by C. R. Hoggatt and R. F. Recht

ABSTRACT—Dynamic uniaxial tensile stress-strain data are obtained at high strain rates by measuring the kinematics of thin-ring specimens expanding symmetrically by virtue of their own inertia. Impulsively loaded to produce high initial radial velocities, expanding rings are decelerated by the radial component of the hoop stresses. Differential equations of motion are evaluated experimentally to obtain the stress-strain (constitutive) relationships which govern the magnitude of these stresses. Techniques have been developed for producing symmetric radial expansion and measuring resulting displacements precisely as a function of time. Dynamic stress-strain relationships have been obtained for 6061-T6 aluminum, 1020 cold-drawn steel, and 6Al-4V titanium. For each of these materials, displacement-time curves are observed to be parabolic within the resolution of the measurements. Results are presented as true-stress/true-strain relationships.

Nomenclature

a = constant
 b = constant
 D = displacement of edge of ring
 D_m = maximum displacement of edge of ring
 E = Young's modulus
 m = mass of ring
 r = internal radius of ring
 r_o = initial internal radius of ring
 R = external radius of ring
 R_o = initial external radius of ring
 \dot{R} = radial velocity of ring
 \ddot{R} = radial deceleration of ring
 t = time

t_m = maximum time
 Z = axial length of ring
 Z_o = initial axial length of ring
 ϵ = true strain
 $\dot{\epsilon}$ = true strain rate
 ν = Poisson's ratio
 ρ = mass density of ring material
 σ = true stress

Introduction

Investigators endeavoring, by experimental means, to determine the constitutive relationships governing the dynamic deformation behavior of metals are confronted by three major problems. (1) A specimen must be loaded so as to produce a desired characteristic stress state in the material being examined. (2) Precise, time-resolved measurement of transient parameters must be accomplished. (3) Data must be correctly interpreted. Impulsive loading produces stress waves. Consequently, when quasi-static test techniques are modified to obtain dynamic stress-strain relationships, wave propagation within the specimen and test-machine component complicate the experiment and the interpretation of results. Nadai and Manjoine used modified conventional tensile-testing techniques to obtain dynamic data.¹ Considerable sophistication has since been added to this approach.² Other investigators are attempting to deduce stress-strain relationships by studying wave propagation in impacted bars.³⁻⁶ The split-Hopkinson-bar technique involves placing a compression specimen between two high-strength bars. An elastic wave is transmitted through the driver bar to the specimen which deforms plastically.

C. R. Hoggatt is Research Engineer and R. F. Recht is Senior Research Engineer and Associate Professor, Denver Research Institute of the University of Denver, Denver, Colo.

Paper was presented at 1969 SESA Spring Meeting held in Philadelphia, Pa., on May 13-16.

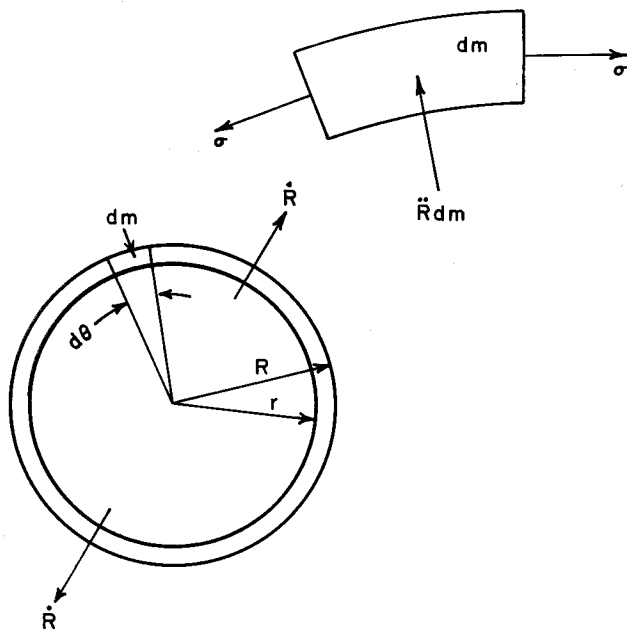


Fig. 1—Dynamic symmetrical expansion of thin ring. Zero internal pressure

Stress-strain relationships are deduced by examining surface strain wave forms obtained from the high-strength bars.⁷⁻¹¹ Clark and Duwez have illustrated the serious consequences associated with assuming uniform conditions to exist within dynamically loaded specimens.¹² Such assumptions can result in exceptionally large errors. The use of short specimens to overcome this difficulty leads to loading geometries which often impose undesired stress states. Obviously, results obtained using these techniques are subject to interpretation. To date, published stress-strain relationships are inconsistent: some investigators observe significant strain-rate effects in a given material; others observe such effects to be quite insignificant.

Symmetrical expansion of thin rings, tubes or spherical shells offers a means to produce uniform deformation in a specimen, avoiding the problem of wave propagation. In 1950, Clark and Duwez dynamically expanded thin tubes filled with mercury through axial impulsive loading of the mercury.¹² Their test is limited to strain rates below 200 in./in./sec by the wave-propagation velocity in the mercury fluid. More recently, Johnson, Stein and Davis devised a means to expand thin rings symmetrically at high strain rates.¹³ Stress-strain results obtained from their experiments suffer due to insufficient resolution in their kinematic measurements.

Experimental Concept

Precise differential equations of motion can be written for thin rings, tubes or spherical-shell speci-

mens which are expanding symmetrically. Utilizing techniques introduced by Johnson, Stein and Davis, short-time impulsive radial loads are applied internally to thin ring specimens by propagating a stress wave through a heavy cylindrical steel driver. The expanding ring leaves the driver, internal pressure disappears and the ring continues to expand by virtue of its own inertia. Radial motion is opposed by radial components of the hoop stress, which can be considered the dependent variable in the equation of motion. Providing that symmetrical expansion and ring separation is achieved and verified, and the kinematics of the expanding ring are measured with suitable precision, dynamic uniaxial stress-strain data can be obtained. While associated measurement problems are difficult to solve, the great advantage of this experimental method is that no assumptions are required to interpret the results of the experiment.

Stress and Strain Derivations

A thin-ring specimen, expanding symmetrically, is shown in Fig. 1. Internal pressure is zero and deceleration is the result of the radial components of the hoop stress, σ . The equation of motion ($F = ma$) for a wall element is,

$$-2\sigma(R - r)Z \sin \frac{d\theta}{2} = \rho(R^2 - r^2)Z_0 \ddot{R} \frac{d\theta}{2} \quad (1)$$

where

\ddot{R} = deceleration of the ring, in./sec²

σ = true stress, psi

ρ = mass density, lb-sec²/in.⁴

R = external radius, in.

r = internal radius, in.

Z = axial length of the ring, in.

Equation (1) properly reduced and solved for the hoop stress becomes,

$$\sigma = -\rho \frac{(R_0^2 - r_0^2)}{2(R - r)} \frac{Z_0}{Z} \ddot{R} \quad (2)$$

To render this equation useful, r and Z must be replaced by functions of R so that measurements of R and \ddot{R} will yield experimental values of the stress. Unit strains in the axial and radial directions for an isotropic material will be equal, thus

$$\frac{Z_0}{Z} = \frac{R_0 - r_0}{R - r} \quad (3)$$

The volume of the ring is,

$$\text{Vol} = \pi(R^2 - r^2)Z \quad (4)$$

and for the uniaxial-stress condition,

$$\frac{\text{Vol}}{(\text{Vol})_0} = \left(1 + \frac{\sigma}{E}\right) \left(1 - \frac{\nu\sigma}{E}\right)^2 \quad (5)$$

where

E = Young's modulus, psi

ν = Poisson's ratio

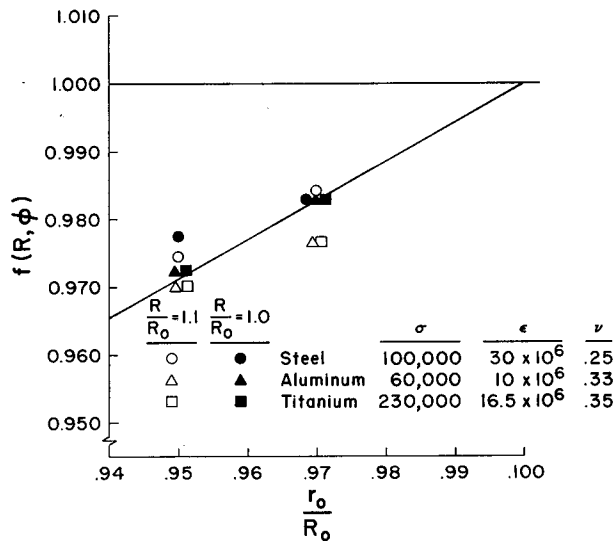


Fig. 2—Ratio of true stress to stress computed by simple formula as a function of ring thickness

Equations (3), (4) and (5) can be combined to obtain,

$$\frac{(R^2 - r^2)(R - r)}{(R_o^2 - r_o^2)(R_o - r_o)} = \left(1 + \frac{\sigma}{E}\right) \left(1 - \frac{\nu\sigma}{E}\right)^2 \quad (6)$$

a cubic equation which when solved for internal radius, r , yields,

$$r = \frac{R}{3} [1 + 4 \cos(\phi/3 + 240^\circ)] \quad (7)$$

where

$$\cos \phi = -1 + \frac{27(R_o^2 - r_o^2)(R_o - r_o)(1 + \sigma/E)(1 - \nu\sigma/E)^2}{16R^3} \quad (8)$$

and

ϕ = an angle lying in the second quadrant (i.e., $\phi \leq 180^\circ$).

Replacing Z_o/Z by eq (3) and r by eq (7) in eq (2) leads to the following equation for true hoop stress in terms of the external radius:

$$\sigma = -\rho R \dot{R} \left\{ \frac{[1 - (r_o/R_o)^2][1 - r_o/R_o]}{8/9(R/R_o)^3 [1 - 2 \cos(\phi/3 + 240^\circ)]^2} \right\} \quad (9)$$

where, for further discussion, the bracketed term is identified as $f(R, \phi)$.

Note that the independent variable appears on the right side of this equation, represented by ϕ . However, it is easily shown that the value of ϕ is insensitive to the value of σ and nominal values for stress can be used to determine the magnitude of $f(R, \phi)$ in the equation. For thin rings, the magnitude of this term is nearly unity as shown in Fig. 2, which compares values of $f(R, \phi)$ for three materials. The plot illustrates that the bracketed term is sensitive to r_o/R_o and is insensitive to differ-

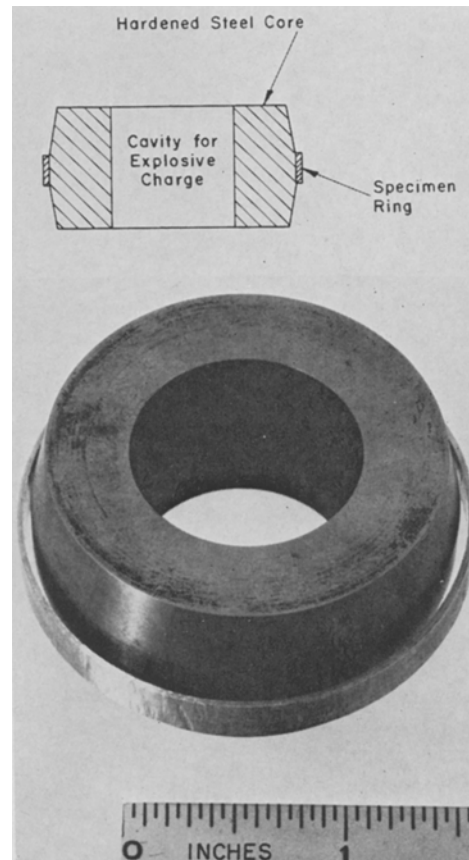


Fig. 3—Schematic drawing and photograph of specimen assembly depicting geometry used in expanding-ring experiments

ences in material properties and to strain as represented by R/R_o . Obviously, for thin rings, the true hoop stress is closely approximated by,

$$\sigma = -\rho R \dot{R} \quad (10)$$

Where experimental resolution is sufficient to justify a more accurate value, the function $f(R, \phi)$ (as presented in Fig. 2) can be applied as a correction factor to this equation to obtain eq (9). A typical value of r_o/R_o is 0.97 which corresponds to a correction factor of about 0.98, a 2-percent reduction in the stress as computed by eq (10).

True (logarithmic) strain is given by,

$$\epsilon = \ln \frac{R}{R_o} \quad (11)$$

from which true strain rate derives as,

$$\dot{\epsilon} = \frac{\dot{R}}{R} \quad (12)$$

Experimental Approach

The specimen geometry used in determining dynamic stress-strain-strain rate relationships is illustrated in Fig. 3. A specimen in the form of a thin ring is shrunk fit onto a hardened-steel core

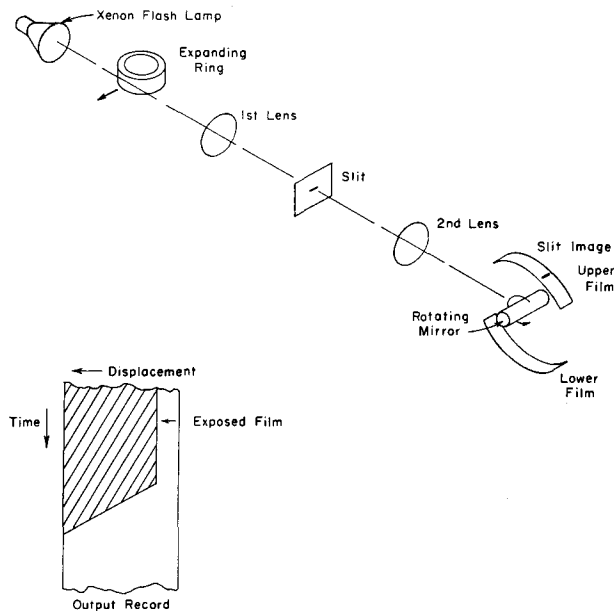


Fig. 4—Streak-camera displacement-measuring system

having a centrally located cavity containing a high explosive charge. Upon detonation of the explosive, a compressive shock wave moves radially outward through the steel. As the shock wave

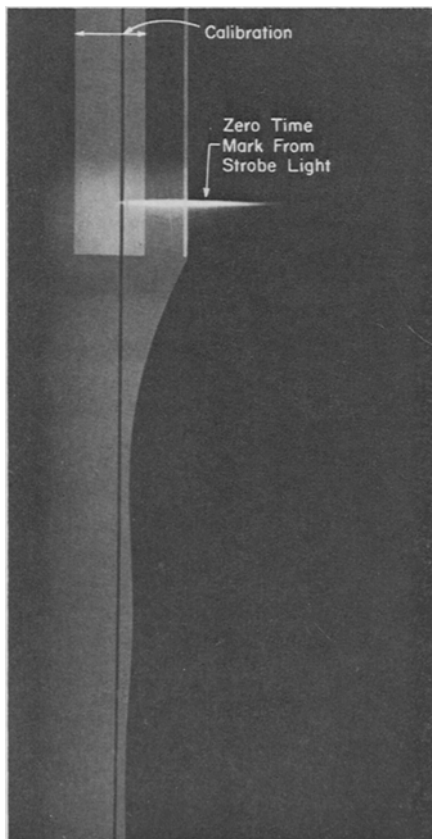


Fig. 5—Streak-camera record for decelerating aluminum ring

reaches the outside surface of the thin ring, it is reflected back as a tensile wave. When the tensile wave arrives at the ring-core interface, the ring separates from the steel core due to the momentum imparted to the specimen. The ring then continues to expand radially by virtue of its own inertia. Monitoring of the displacement-time history of the ring with a high degree of precision following separation provides the information necessary for determining the stress-strain-strain rate relationships of interest.

The continuous displacement-time history of the expanding ring is recorded using a streak camera in conjunction with the optical system depicted in Fig. 4. The quality and size of the optical system is such that lens aberrations and distortions are negligible. In this system, a slit is illuminated through the optical system by a back-lighting technique such that the image of the ring specimen covers a portion of the slit. The specimen is placed so that the displacement to be measured is in the direction of the arrow. The first lens focuses the shadow of the ring at the slit plane. A narrow slit eliminates all but a thin horizontal segment of the light passing the expanding ring. As the ring expands, its shadow progressively covers the slit. A second lens focuses an image of the slit onto a curved film holder via a rotating mirror. As the mirror rotates, the slit image is swept along the film, producing a continuous record of the displacement of the ring as a function of time on the film.

A streak-camera record for a decelerating 6061-T6 aluminum ring is shown in Fig. 5. As presented, the "rest" position of the outer edge of the ring is the straight-line portion of the trace in the upper right side of the figure. During expansion, displacement is to the left and time increases downward. It can be observed in the figure that, after the maximum displacement of the ring has been achieved, some recovery occurs as a result of elastic material behavior (providing the ring has not failed). The elastic ringing associated with this recovery is recorded as the sinusoidal portion of the trace. In the event that failure does occur in the ring, the streak record should exhibit a straight-line portion following fragmentation, due to the fact that the material strength is no longer resisting radial motion and the various pieces of the ring are therefore traveling at an essentially constant velocity. A record of a 6061-T6 aluminum ring loaded to failure is shown in Fig. 6. The constant slope is quite evident.

An illustration demonstrating separation behavior between the ring and the core is shown in Fig. 7. In this figure, the lower trace is a displacement-time record obtained by observing an expanding ring during a normal experiment; the upper trace is a displacement-time record obtained by eliminating the ring specimen and observing the radial motion of the hardened-steel core itself during an identical test.

The displacement-time record obtained from the AVCO streak camera is read at selected increments of time using an enlarging technique which provides a readout resolution for displacement that approaches 0.0005 in. This is accomplished by placing the film record (already at a $\times 2$ magnification) directly into a microfilm-type enlarger and enlarging the displacement-time trace an additional ten times (total magnification being $\times 20$). Standard grid patterns were used to establish that the magnified image was not being distorted as a result of the enlarging technique. The enlarged displacement-time record and the calibration width are then precisely traced, selected increments of time marked on the trace, and corresponding values of displacement are measured.

During the development of the experimental techniques required to (1) obtain symmetrical expansion and (2) measure displacement precisely as a function of time, another paper was published describing the means employed to verify symmetry and accuracy.¹⁴ A detailed account of the experimental schemes and related instrumentation was presented therein.

Analysis of the Data

Early in the program, curve-fitting techniques were evaluated as a means for reducing the displacement-time and velocity-time data into dynamic stress-strain relationships. Initial attempts involved computerized techniques utilizing third- and fourth-order polynomial fits to the data. The data were smoothed using the method of fourth differences and differentiation of empirical functions performed in accordance with methods given by Lanczos.¹⁵ Very limited success was achieved with this approach due to characteristic frequencies produced as a result of single and especially double differentiation of third- and fourth-order polynomials. The amplitude of the frequency response was of sufficient magnitude to produce wide extremes in the second differential, masking true material behavior. This approach and the difficulties encountered have been described by the authors in the paper previously cited.¹⁴

After a number of experiments had been performed, close examination of the data revealed that

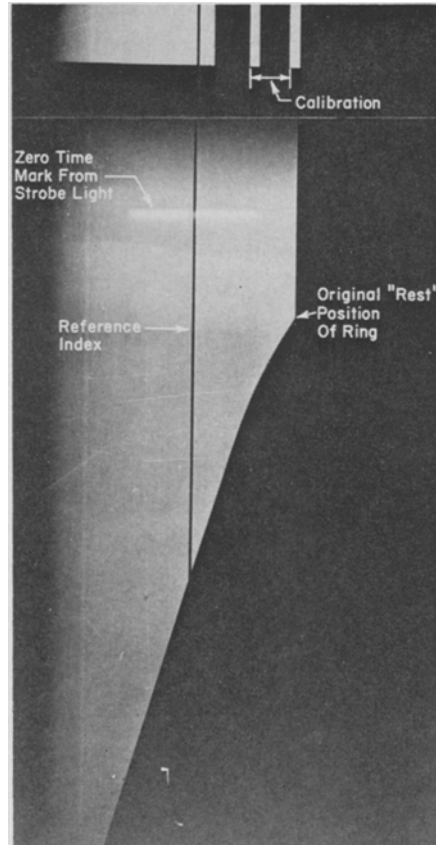


Fig. 6—Streak-camera record for decelerating aluminum ring illustrating ring fracture

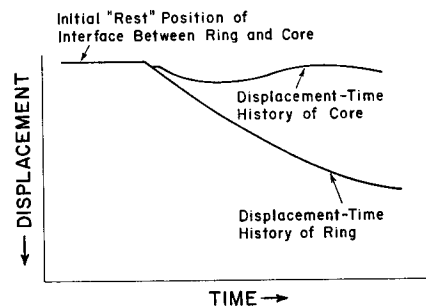


Fig. 7—Illustration of separation behavior between ring and core

TABLE 1—ILLUSTRATION OF DEGREE OF DEVIATION BETWEEN MEASURED DISPLACEMENTS AND DISPLACEMENTS CALCULATED FROM PARABOLIC RELATIONSHIPS

—1020 Cold-drawn steel—				—6Al-4V Titanium—				—6061-T6 Aluminum—			
Displacement, in.		Time (μ sec)		Displacement, in.		Time (μ sec)		Displacement, in.		Time (μ sec)	
Meas.	Calc.			Meas.	Calc.			Meas.	Calc.		
Shot # 69	0.0308	0.0310	10	Shot # 71	0.0154	0.0159	3	Shot # 78	0.0387	0.0381	10
	0.0736	0.0737	30		0.0266	0.0271	6		0.0499	0.0499	15
	0.0853	0.0855	40		0.0333	0.0334	9		0.0568	0.0569	20
Shot # 67	0.0380	0.0381	10	Shot # 72	0.0284	0.0279	4	Shot # 79	0.0695	0.0695	10
	0.0948	0.0947	30		0.0471	0.0474	8		0.0956	0.0959	15
	0.1251	0.1252	50		0.0581	0.0585	12		0.1168	0.1168	20

displacement-time histories appeared to obey simple parabolic relationships. Parabolic behavior proved to be characteristic for all materials tested from initial movement out to 12-percent strain, which is the maximum strain achieved to date. (Failure was produced in 6061-T6 aluminum at this strain.) Maximum deviation of the recorded data from parabolic behavior at any position on the curve was seldom greater than the readout resolution attainable on displacement, i.e., approximately 0.0005 in. This held true for all three materials tested, (6061-T6 aluminum, 1020 cold-drawn mild steel, and 6Al-4V titanium). Typical illustrations of the degree of deviation encountered are presented in Table 1. It should be noted that these materials represent three different crystal structures (face-centered cubic, body-centered cubic and hexagonal close packed); three ranges of material density (0.25×10^{-3} , 0.733×10^{-3} and 0.414×10^{-3} lb-sec²/in.⁴); and three ranges of dynamic material strength (50, 100 and 225 ksi). Even with such a wide variance of conditions, investigations to date indicate that the parabolic relation for displacement-time behavior holds for all materials tested, and the dynamic stress-strain relationships obtained agree quite well with data obtained by some of the more prominent investigators in the field.^{10-13, 16-21}

Fitting a parabola to the displacement-time trace is accomplished by establishing the point of maximum displacement, D_M , on the film trace as the apex of a parabola having a vertical axis of symmetry and displaced a distance, b , from the x axis as shown in Fig. 8. The form of this parabola is represented as:

$$D = at^2 + b \quad (13)$$

where

$$b = -D_M$$

and since $D_M = -at_M^2$ it follows that $a = -D_M/t_M^2$.

Time is measured from the onset of initial displacement (the 0,0 origin shown in the figure); therefore, the actual time is expressed as $t_M - t$.

Substituting into eq (13) gives

$$\begin{aligned} D &= a(t_M - t)^2 + b \\ D &= at_M^2 - 2att_M + at^2 + b \\ D &= \frac{-D_M t_M^2}{t_M^2} + 2 \frac{D_M t t_M}{t_M^2} - \frac{D_M t^2}{t_M^2} - D_M \end{aligned}$$

or

$$D = \frac{2D_M t}{t_M} - \frac{D_M t^2}{t_M^2} \quad (14)$$

Equation (14) is the expression used to calculate the displacement at any point along the parabola by assuming a value of time and obtaining the maximum displacement and time values from the film trace. Having verified the parabolic fit to the displacement-time data, constants can be

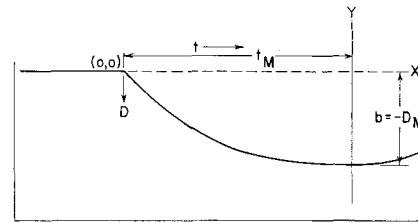


Fig. 8—Orientation of film trace for fitting a parabolic curve

evaluated for each test and eq (14) differentiated once to obtain the velocity of the expanding ring, and twice to obtain its deceleration, i.e.,

$$\dot{R} = \frac{2D_M}{t_M} - \frac{2D_M t}{t_M^2} \quad (15)$$

and

$$\ddot{R} = -\frac{2D_M}{t_M^2} \quad (16)$$

By the very nature of the experiment, the strain rate to which the material is subjected decreases continuously throughout the duration of the test. To obtain meaningful stress-strain-strain rate behavior from a test such as this, it becomes necessary to determine the values of stress corresponding to various values of strain for a constant-strain-rate condition. The manner in which data of this nature is correlated is illustrated in Fig. 9. In this figure, it can be observed that both stress and strain rate are plotted against strain for eight separate expanding-ring tests. To obtain a typical dynamic stress-strain curve, a value of strain rate is selected and by moving across the plot horizontally, various values of strain are determined from intersections with the strain-strain rate curves. By moving vertically upward from each established value of strain, the corresponding value of stress is established by intersecting the stress-strain curve for each test conducted. While any one test provides a series of data points, only one data point per strain-rate value can be obtained. For this reason,

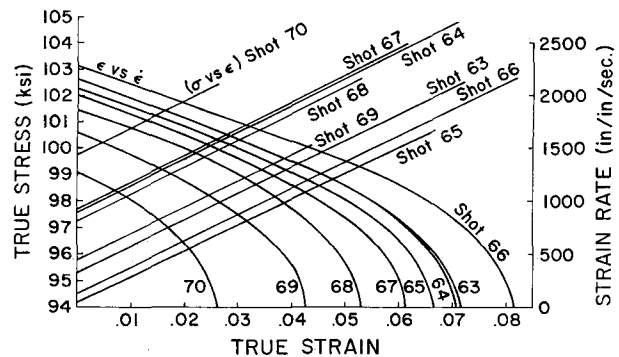


Fig. 9—Data-correlation plot for obtaining stress-strain-strain rate relationships for 1020 cold-drawn steel

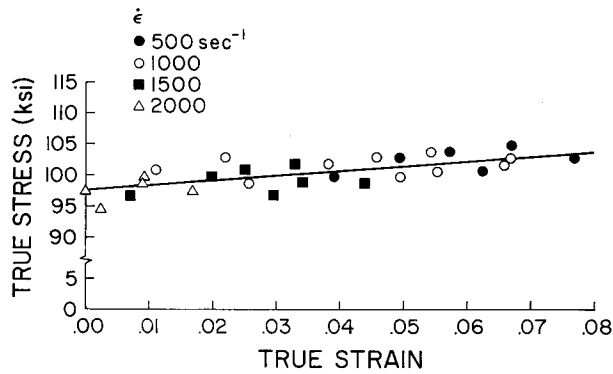


Fig. 10—Dynamic stress-strain relationship for 1020 cold-drawn steel

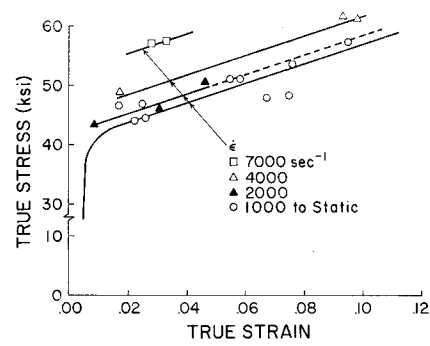


Fig. 12—Dynamic stress-strain relationships for 6061-T6 aluminum

a series of tests conducted at varying initial strain rates (such as the eight curves in Fig. 9) are required to define material behavior under conditions of constant strain rate. Several approaches can be taken to vary the initial strain rate to which the ring is subjected; i.e., varying (1) quantity of explosive used, (2) diameter of central hole in core, and (3) overall diameter of the ring and core assembly. Changes in any of these parameters influences the initial separation velocity of the ring and thereby the strain rate and maximum displacement. While effects of prior strain-rate history on the specimen might be expected to influence dynamic behavior for certain materials, no such influence has been observed on the materials tested.

Dynamic Stress-Strain Relationships

Dynamic stress-strain relationships have been determined for 1020 cold-drawn steel, 6Al-4V titanium, and 6061-T6 aluminum. Maximum strain rates were of the order of 0.8×10^4 in./in./sec. These results, obtained using the expanding-

ring technique, are presented in Figs. 10, 11 and 12. Dynamic stress values reported in Figs. 10 and 11 for 1020 cold-drawn steel and 6Al-4V titanium, respectively, are considerably greater than static values. Approximate values of static yield and flow stress (at 5-percent strain) for the steel alloy are 60 and 80 ksi and, for the titanium alloy, are 136 and 170 ksi. Within the strain-rate range considered in these tests (500 to 2000 sec^{-1} for steel and 100 to 8000 sec^{-1} for titanium) the stress-strain relations for both of these materials tend to be represented by a single dynamic curve. On the other hand, the dynamic stress-strain curve for 6061-T6 aluminum is essentially the same as the static curve until a strain rate in excess of 10^3 in./in./sec is attained (see Fig. 12). Appreciable values of static yield and flow stress at 5-percent strain are 40 and 49 ksi. Above this strain rate, appreciable increases in flow stress were observed.

Due to variations in experimental technique and interpretation of experimental results, published stress-strain relationships obtained by various investigators for a given material often exhibit marked differences. Until these anomalies are

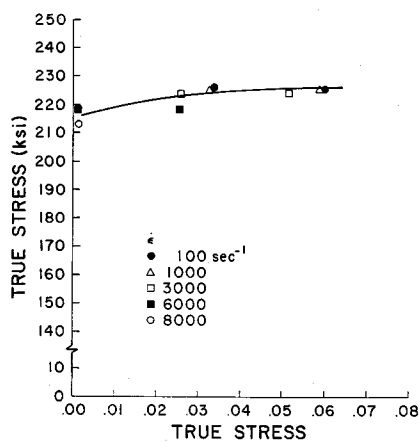


Fig. 11—Dynamic stress-strain relationship for 6Al-4V titanium

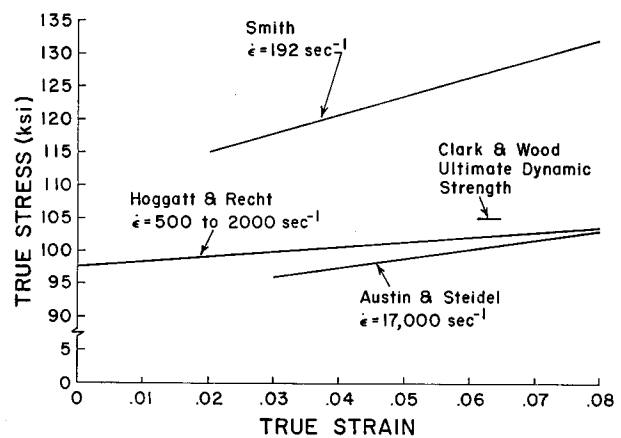


Fig. 13—Comparison of dynamic stress-strain relationships for 1020 cold-drawn steel

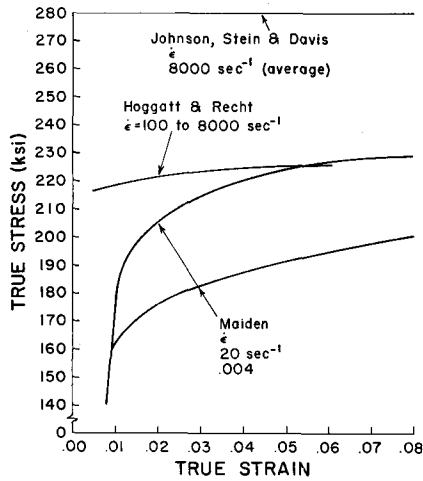


Fig. 14—Comparison of dynamic stress-strain relationships for 6Al-4V titanium

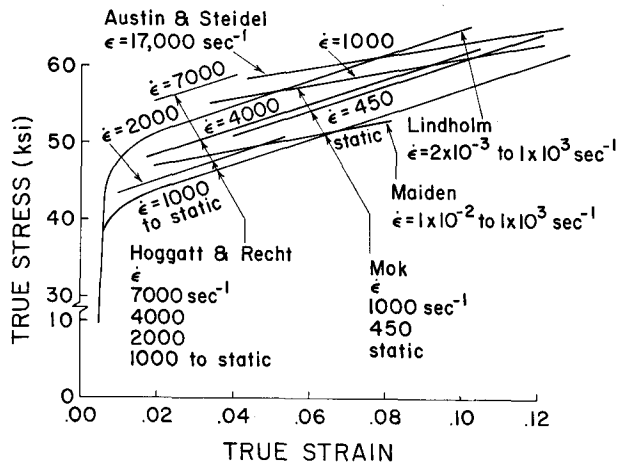


Fig. 15—Comparison of dynamic stress-strain relationships for 6061-T6 aluminum

resolved, it will not be possible to combine data obtained from several sources to establish generalized stress-strain behavior. Results of the expanding-ring experiments are compared to results obtained by other means in Figs. 13, 14 and 15.

Conclusions

Dynamic symmetrical free expansion of thin rings offers a valid means for obtaining uniaxial tensile stress-strain relationships at high strain rates. Rings can be impulsively loaded so that they will continue to expand against the resistance of the hoop stresses by virtue of their radial inertia, the internal pressure being zero. Provided that symmetry is preserved, the accuracy of the experiment corresponds to the accuracy of the determination of instantaneous acceleration (deceleration) values. Displacement-time relationships

for the materials tested were observed to be parabolic (maximum deviations from the parabolic fit being of the same magnitude as the readout resolution attainable on the displacement measurement). Consequently, exact differentiations can be performed to obtain the deceleration behavior of the ring and the resulting dynamic stress-strain relations. The greatest single advantage of the expanding-ring technique is that no interpretation of the data is required if the experiment is properly conducted. Results can be directly evaluated in terms of true stress and natural strain.

Acknowledgments

The authors wish to acknowledge the assistance of William Orr, who devised much of the experimental instrumentation, and James Dunn and Roy Hatfield, who conducted the experimental work. This work was performed under Contract DA 12-066-AMC-266(X) which is supporting a center for High Energy Forming, a joint effort of the Martin Co. and the University of Denver.

References

1. Nadai, A., *Theory of Flow and Fracture of Solids, I*, McGraw-Hill, Inc., N. Y. (1950).
2. Krafft, J. M., "Response of Metals to High Velocity Deformation," *Proc. AIME, Metallurgical Society Conferences* (1960).
3. Johnson, J. E., Wood, D. S. and Clark, D. S., "The Dynamic Stress-Strain Relation of Annealed 2S Aluminum Under Compression Impact," *Trans. ASME* (1953).
4. Kolsky, H., "The Propagation of Mechanical Pulses in Anelastic Solids," *Proc. ASME Colloquium on the Behavior of Materials Under Dynamic Loading, 1* (November 1965).
5. Bell, J. F., "The Dynamic Plasticity of Metals at High Strain Rates—An Experimental Generalization," *Proc. ASME Colloquium on the Behavior of Materials Under Dynamic Loading, 19* (November 1965).
6. Ripperger, E. A., "Dynamic Plastic Behavior of Aluminum, Copper and Iron," *Proc. ASME Colloquium on Behavior of Materials Under Dynamic Loading, 62* (November 1965).
7. Dorn, J. E., Hauser, F. E. and Simmons, J. A., "Strain Rate Effects in Plastic Wave Propagation," No. 9, *Response of Metals to High Velocity Deformation, Proc. AIME Metallurgical Society Conferences*, (1960).
8. Malvern, L. E., "Experimental Studies of Strain Rate Effects and Plastic Wave Propagation in Annealed Aluminum," *Proc. ASME Colloquium on the Behavior of Materials Under Dynamic Loading, 81* (November 1965).
9. Lindholm, U. S., "Dynamic Deformation of Metals," *Proc. ASME Colloquium on the Behavior of Materials Under Dynamic Loading, 42* (November 1965).
10. Kumar, A., Maiden, C. J. and Green, S. J., "Survey of Strain Rate Effects," *Proc. First Intl. Conf. Center for High Energy Forming* (June 19-23, 1967).
11. Maiden, C. J. and Green, S. J., "Compressive Strain Rate Tests on Six Selected Materials at Strain Rates from 10^{-3} to 10^4 in./in./sec.," *Jnl. Appl. Mech.* (September 1966).
12. Clark, D. S. and Duwez, P. E., "The Influence of Strain Rate on Some Tensile Properties of Steel," *Proc. ASTM*, **50**, 1 (1950).
13. Johnson, P. C., Stein, B. A. and Davis, R. S., "Basic Parameters of Metal Behavior Under High Rate Forming," *Final Report WAL TR 111 2/20-6* (Contract DA-19-020-ORD-5239), Arthur D. Little Corp. for Watertown Arsenal (1962).
14. Hoggatt, C. R. and Recht, R. F., "The Use of an Expanding Ring for Determining Tensile Stress-Strain Relationships as Functions of Strain Rate," *Proc. First Intl. Conf. Center for High Energy Forming, Estes Park* (June 19-23, 1967).
15. Lanczos, C., *Applied Analysis*, Prentice-Hall (1956).
16. Mok, C. H. and Duffy, J., "The Dynamic Stress-Strain Relation of Metals as Determined from Impact Tests with a Hard Ball," *Brown Univ. Rept. Nonr-562*(20)137 (June 1964).
17. Hoge, K. G., "Influence of Strain Rate on Mechanical Properties of 6061-T6 Aluminum Under Uniaxial and Biaxial States of Stress," *EXPERIMENTAL MECHANICS*, **6** (4), 204-211 (1966).
18. Clark, D. S. and Wood, D. S., "The Tensile Impact Properties of Some Metals and Alloys," *Trans. ASM*, **42** (1950).
19. Austin, A. L. and Steidel, Jr., R. F., "A Method for Determining the Tensile Properties of Metals at High Rates of Strain," *Proc. SESA*, **XVII** (1), 99-114 (1959).
20. Smith, J. E., "Tension Tests of Metals at Strain Rates up to 200 sec.⁻¹" *Mails. Res. and Stand.* (September 1963).
21. Lindholm, U. S. and Yeakley, L. M., "High Strain-rate Testing: Tension and Compression," *EXPERIMENTAL MECHANICS*, **8** (1), 1-9 (1968).